Structure and magnetic properties of rf thermally plasma synthesized Mn and Mn–Zn ferrite nanoparticles

S. Son,[a] R. Swaminathan, and M. E. McHenry
Department of Materials Science and Engineering, Carnegie Mellon University, Pittsburgh, Pennsylvania 15213

(Presented on 13 November 2002)

Plasma synthesis has previously been shown to be a viable route to producing nanocrystalline magnetite and Ni ferrite nanoparticles. In this work nanocrystalline powders of Mn and Mn–Zn ferrites have been synthesized using a 50 kW–3 MHz rf (radio frequency) induction plasma torch. We investigate these materials for soft magnetic applications. High-energy ball milled Mn + Fe powders and (Mn+Zn) +Fe powders (<10 μm) in the stoichiometric ratio of 1:2 were used as precursors for the ferrite synthesis. Compressed air was used in the oxygen source for oxidation of metal species in the plasma. X-ray diffraction patterns for the plasma-torched Mn ferrite and MnZn ferrite powders were indexed to the spinel ferrite crystal structure. An average grain size of ~20 nm was determined from Scherrer analysis confirmed by transmission electron microscopy studies. The particles also exhibited faceted polygonal growth forms with the associated truncated cuboctahedral shapes. Room-temperature vibrating sample magnetometer measurements of the hysteretic response revealed saturation magnetization M_s and coercivity H_c of Mn ferrite are 23.65 emu/g and 20 Oe, respectively. The Néel temperatures of Mn ferrite powders before and after annealing (500 °C, 30 min) were determined to be 200 and 360 °C, respectively. Inductively coupled plasma chemical analysis and energy dispersive x-ray analysis data on the plasma-torched powders indicated deviations in the Mn or Zn contents than the ideal stoichiometry. MnZn ferrite was observed to have a Néel temperature increased by almost 400 °C as compared with as-synthesized Mn ferrite but with a larger coercivity of ~35 Oe. © *2003 American Institute of Physics.* [DOI: 10.1063/1.1557953]

In recent years, as electronic devices have become more miniaturized, offering increasingly high levels of performance, the trend has been towards much higher-signal frequencies. Ferrites have been of great importance in high-frequency soft magnetic applications owing to their large resistivities, low power losses, and high permeabilities. Mn ferrites and MnZn ferrites have especially come to light as essential materials for higher-frequency (up to MHz) applications such as inductors, transformers, and yoke coils.[1–3]

Mn ferrites and MnZn ferrites possessing the cubic spinel structure are described by the formula $(A)[B]_2O_4$ where (A) and [B] refer to tetrahedral and octahedral cation sites, respectively, in a face-centered cubic anion (oxygen) sublattice. The type of cations and their distribution between the two interstitial sites in these ferrites determine many of the intrinsic magnetic properties of the ferrites.[4] Interestingly, some nanocrystalline spinel ferrites show different cation distributions and, as a consequence, diverse resulting magnetic properties when compared with their bulk counterparts.[5,6] It should be noted that the equilibrium distribution of cations in the spinel structure depends on ionic radii, electronic configuration, electrostatic energies, and polarization effects. However, using non-equilibrium processing routes, one can achieve nonequilibrium distribution of cations in the spinel ferrites.[7]

rf inductively coupled plasma synthesis has been previously shown to be a viable route to producing nanocrystalline magnetite and Ni ferrite nanoparticles.[8] In this study, our goal is to produce nanocrystalline Mn ferrites and MnZn ferrites from metallic precursors by rf plasma torch synthesis and characterize their structural and magnetic properties.

Two types of precursor samples were prepared for plasma synthesis. Precursor sample 1 was a mixture of pure Mn (<45 μm) powder and pure Fe powder (6–10 μm) at the atomic ratio of 1:2 (i.e., that of the desired cation ratio). Sample 2 was a mixture of Mn, pure Zn dust (<10 μm), and Fe with overall Mn:Zn:Fe ratio=1:1:4. Both samples 1 and 2 were ball milled for two hours using a high-energy ball mill (SPEX 800M Mixer/Mill, SPEX CertiPrep Inc.) to ensure homogeneous mixing.

An rf induction thermal plasma system consisting of a TEKNA PL50 type plasma torch head with a 50 kW, 3 MHz power supply was used for producing the nanocrystalline ferrite powders with the ball-milled metallic precursor samples. Argon gas was used as the plasma gas and the plasma sheath gas consisted of a mixture of Ar and H_2 gas. All the precursor powder was injected through the plasma jet stream by Ar, a carrier gas. After the induction plasma was established, compressed air was introduced into the reactor as an oxidizer. More detailed processing procedures can be found elsewhere.[9,10]

X-ray diffraction (XRD) of both the precursor powders and the as-synthesized powders were performed on a Rikagu diffractometer using Cu K_α radiation (λ=1.54 Å). Scanning

[a]Electronic mail: sson@andrew.cmu.edu

 © 2003 American Institute of Physics

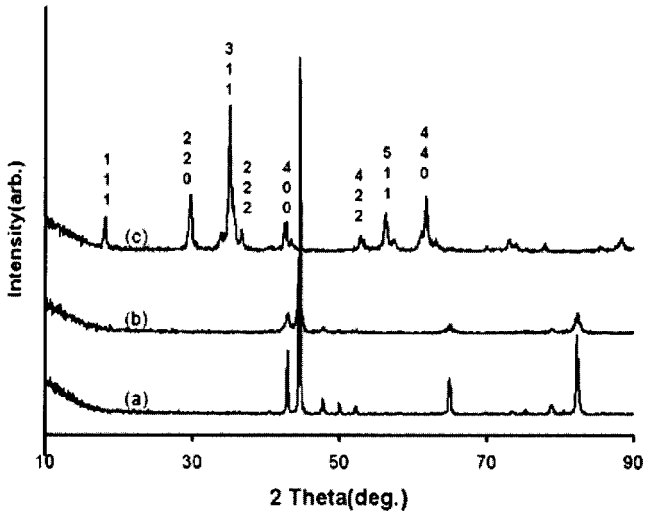

FIG. 1. X-ray diffraction patterns: (a) Mn+Fe raw powder; (b) Mn+Fe ball-milled powder; and (c) plasma-torched Mn ferrite powder.

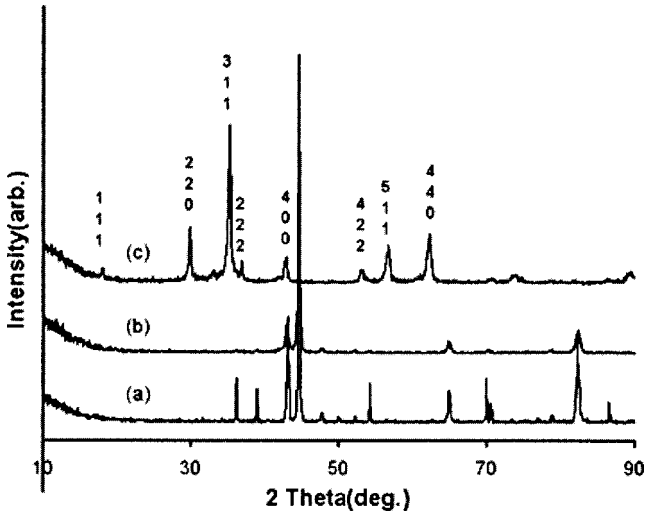

FIG. 2. X-ray diffraction patterns: (a) Mn+Zn+Fe raw powder; (b) Mn +Zn+Fe ball-milled powder; and (c) plasma-torched MnZn ferrite powder.

electron microscopy (Philips XI-30 FEG model) and high-resolution transmission electron microscopy (TECNAI F20 model) with energy dispersion x-ray (EDX) and electron energy-loss spectroscopy (EELS) were used to examine the morphology and composition of particles. The chemistry of the ferrites was further studied by inductive coupled plasma (ICP) chemical analysis (Perkin-Elmer Optima 2000DV ICP-OES). The magnetic properties of the samples were obtained with a high-temperature vibrating sample magnetometer (VSM; Lake Shore Model 7300, with 1000 °C oven assembly).

The formation of nanoparticles in the gas phase involves the reaction of a supersaturated metal vapor with the oxygen containing species and rapid cooling to room temperature by the cold inert gas (Ar) or further on the surface of water-cooled chamber. Hence, this kind of processing is inherently nonequilibrium. At the extreme temperatures in the plasma jet, vaporized metal atoms react with oxygen and are cooled rapidly, forming ferrite embryos within a very short time interval. In this supercritical region, numerous nuclei or embryos formed coalesce together, forming the stable nuclei from the embryos. The growth of the particles stops when they travel out of the growth zone where there is no further supply of atoms, embryos, or nuclei. The temperatures in the growth zone are high. Finally, the particles are quenched by a cooled solid substrate that is a wall of reactor and metal filter. The temperature difference between the plasma plume and the cooled substrate has been estimated to be a few thousand Kelvin.[10] The ferrite nanoparticles are collected at room temperature.

Figures 1 and 2 show the XRD patterns of samples 1 and 2, respectively. After high-energy ball milling, the diffraction peaks broadened [(a) versus (b) in both figures], which indicated that the ball-milled particle size was significantly reduced as compared with that of the mixture of precursor powders. XRD peaks on plasma-torched powders revealed that most of the metallic precursor powders were transformed into nanocrystalline ferrites. All major peaks were indexed to the standard pattern for Mn ferrite and MnZn ferrite, respectively. The average particle size of as-produced ferrite powder was estimated from the Scherrer formula.[11] The (311) ferrite peak was chosen for calculating the average particle size. The Scherrer analysis showed that the average grain size of all the samples were reduced from ~10 μm starting powder size to ~20 nm after plasma synthesis; Mn ferrite and MnZn ferrite samples have an average size of about 15 and 21 nm, respectively. TEM analysis of 346 randomly selected Mn ferrite particles shows that the average size is 9.2 nm and standard deviation is 9.2 nm. MnZn ferrite has an average size of 9.6 nm in TEM analysis of 385 randomly selected particles and its standard deviation is 10 nm. ICP analysis on both samples indicated that the powders did not result in full stoichiometric alloying after the plasma synthesis. The EDX results showed that we were able to synthesize MnZn ferrites close to the stoichiometric $Mn_{0.5}Zn_{0.5}Fe_2O_4$, but the Mn ferrites were off stoichiometry ($MnFe_2O_4$) (Table I).

TEM observations of the ferrite nanoparticles revealed the faceting with polygonal growth forms, most of them exhibiting (111) faceting with truncated cuboctahedral shapes (Fig. 3). For picturing polygonal faceting in the synthesized powders, EELS is a good tool which has the capability of

TABLE I. Physical properties of the as-produced ferrite particles.

	Mn ferrite	MnZn ferrite
Average particle size (nm)	15	21
Lattice parameter (Å)	~8.45	~8.42
ICP result (at. %)	Fe 56.82 and Mn 40.89[a]	Fe 78.1, Zn 17.6, and Mn 4.3
	Fe 74.1 and Mn 25.9	Fe 80, Zn 16.3, and Mn 3.7
EDX result (at. %)		Fe 76.66, Zn 18.75, and Mn 4.59
Coercivity, H_c (Oe)	20	35
Saturation magnetization M_s (emu/g)	23.6	47.1
Néel temperature (°C)	200	600

[a]There is also 2.3 at. % Ni in the Mn ferrite.

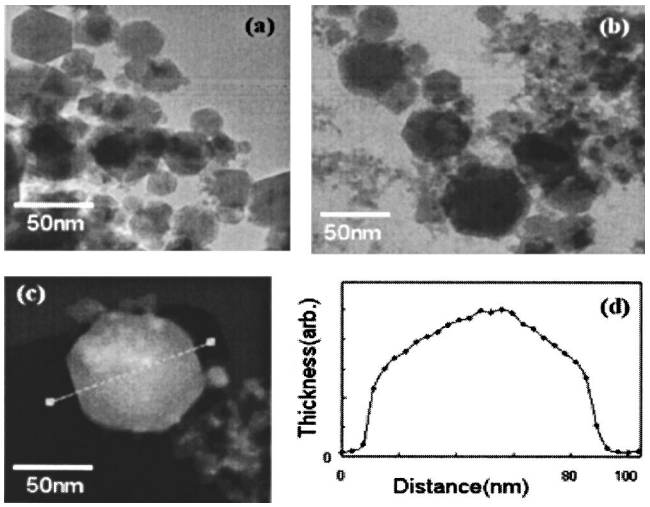

FIG. 3. TEM images: (a) Mn ferrite particles; (b) MnZn ferrite particles; and (c) and (d) EELS thickness profile of Mn ferrite particles.

getting the thickness profile of particles. EELS spectrum shows the energy loss due to both elastic and inelastic scatterings in TEM. Since the amount of all inelastic scattering increases with the specimen thickness, one can get the thickness profile of the particle by measuring the ratio of zero-loss peak intensity to total intensity in the spectrum.[12] The determination of thickness profile using EELS is shown in Fig. 3(d).

For faceted particles with cubic symmetry and with exclusively (100) and (111) faces, the possibilities for particle morphologies include cube, octahedron, truncated cube, truncated octahedron, and cuboctahedron (Fig. 4). In our observations, we seldom see perfect cubes or octahedra and an energetic argument (to be published later) shows that the perfect cuboctahedron is also rare. We thus categorized the particles by the frequency of occurrence of the truncated cubic and truncated octahedral shapes at different particle sizes. The degree of truncation describes the fraction of (100) and (111) faces in any particle (Fig. 5). In both Mn ferrites and Mn–Zn ferrites, in the size range of 12–32 nm, we see primarily truncated octahedra, which are seen in the TEM micrographs as six-sided figures (which are projections of a truncated octahedron along the ⟨111⟩ direction). In the size range >12 nm, in the case of Mn–Zn ferrite we see more of the truncated cubes (eight-sided polygons when projected along the ⟨100⟩ direction) than the truncated octahedron and exactly the opposite in the case of Mn ferrite. This analysis is

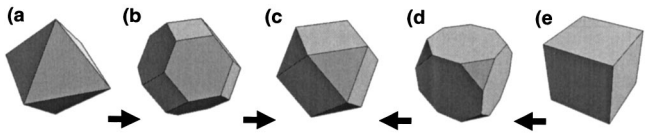

FIG. 4. Truncation of cube and octahedron: (a) octahedron; (b) truncated octahedron; (c) perfect cuboctahedron; (d) truncated cube; and (d) cube.

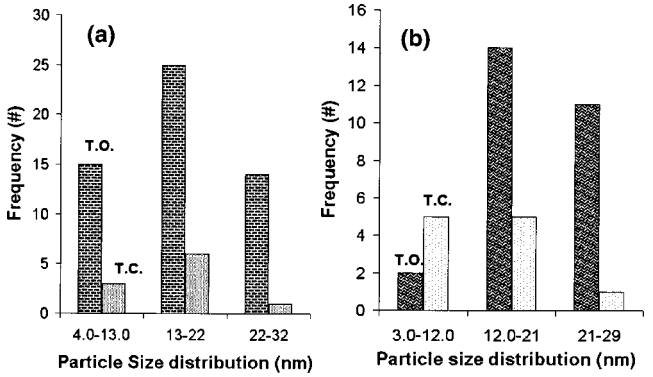

FIG. 5. Shapes and size distribution of (a) Mn ferrite particles and (b) MnZn ferrite particles (T.O.: truncated octahedron, T.C.: truncated cube).

important since (100) and (111) faces in the ferrite structure are terminated by different polyhedra and the degree of truncation determines the surface anisotropy.

Magnetic hysteresis and magnetization versus temperature curves were measured using VSM at room temperature. Coercivities values H_c and Néel temperatures of both ferrites are shown in Table I. The saturation magnetization M_s and the coercivity H_c of Mn ferrite are 23.6 emu/g and 20 Oe, respectively. The Néel temperature of as-produced Mn ferrite is around 200 °C. It is interesting to know that after furnace annealing of the powder at 500 °C for 30 min in open atmosphere, the Néel temperature became 360 °C. The change of Néel temperature might be ascribed to the cation redistribution through heating process.

Our results clearly demonstrate the viability of plasma torch synthesis for production of ferrite nanoparticles as did the previous report on Ni ferrite synthesis.[7] Still more research such as using alloy powder for precursor, controlling of atmosphere in the reaction chamber and thermodynamic calculation of oxide formation will be required for optimum control of the stoichiometry of the particles.

The authors thank T. Nuhfer and T. Ohkubo for helping with TEM analysis. E.E. Carpenter is gratefully acknowledged for the ICP results. This work was sponsored by the Air Force Of Scientific Research, Air Force Material Command, USAF, under Grant No. F49620-96-0454.

[1] M. Sugimoto, J. Am. Ceram. Soc. **82(2)**, 269 (1999).
[2] K. Ono *et al.*, *Proceedings 8th International Conference Ferrites, Kyoto and Japan,* (2000), pp. 13–15.
[3] P. I. Slick, in *Ferromagnetic Materials: A Handbook on the Properties of Magnetically Ordered Substances*, edited by E. P. Wohlfarth (North-Holland, Amsterdam, 1980), Vol. 2, Chap. 3, pp. 191–199.
[4] E. C. Snelling, *Soft Ferrites: Properties and Applications* (Butterworths, London, 1988), p. 1–7.
[5] D. J. Fatemi *et al.*, J. Appl. Phys. **85(8)**, 5172 (1999).
[6] C. Rath *et al.*, J. Appl. Phys. **91(4)**, 2211 (2002).
[7] T. Seshagiri Rao, in *Ferrite Materials–Science & Technology,* edited by B. Viswanathan and V. R. K. Murthy (Narosa, 1990), Chap. 1, pp. 2–17, and Chap. 3, pp. 39–50.
[8] S. Son *et al.*, J. Appl. Phys. **91(10)**, 7589 (2002).
[9] Z. Turgut, Ph.D. thesis, CMU 2000.
[10] M. I. Boulos J. High Temp. Chem. Processes **1**, 401 (1992).
[11] B. D. Cullity, *Elements of X-ray Diffraction*, 2nd ed. (Addison-Wesley, Reading, MA, 1978), pp. 101–102.
[12] D. B. Williams and C. B. Carter, *Transmission Electron Microscopy: A Textbook for Materials Science* (Plenum, New York, 1996), pp. 678–679.